Frontiers of Optoelectronics (2024) 17:15
https://doi.org/10.1007/s12200-024-00120-8

Frontiers of Optoelectronics

COMMUNICATION

Circularly polarized light emission and detection by chiral inorganic semiconductors

Zha Li[1] · Wancai Li[2] · Dehui Li[2] · Wei Tang[3,4] · Huageng Liang[5] · Huaibing Song[6] · Chao Chen[2] · Liang Gao[1] · Jiang Tang[1,2]

Received: 17 February 2024 / Accepted: 16 April 2024

Abstract
Chiral inorganic semiconductors with high dissymmetric factor are highly desirable, but it is generally difficult to induce chiral structure in inorganic semiconductors because of their structure rigidity and symmetry. In this study, we introduced chiral ZnO film as hard template to transfer chirality to $CsPbBr_3$ film and PbS quantum dots (QDs) for circularly polarized light (CPL) emission and detection, respectively. The prepared $CsPbBr_3$/ZnO thin film exhibited CPL emission at 520 nm and the PbS QDs/ZnO film realized CPL detection at 780 nm, featuring high dissymmetric factor up to around 0.4. The electron transition based mechanism is responsible for chirality transfer.

Keywords High dissymmetric factor · Circularly polarized light emission · Semiconductor · Hard template · Chirality

1 Introduction

Circularly polarized light (CPL) intrigues increasing attention for diverse applications, including 3D display, sensor, information storage, and etc. [1–4]. The CPL can be obtained by optical waveplates, but the use of waveplates is not beneficial to integrated devices. Thus, the exploration of novel materials and structures with the ability of CPL emission and detection is significative. Chiral organic molecules have demonstrated superior performance of CPL emission and detection, while the organic molecules suffer from the instability and low dissymmetry factors [5]. Generally the chiral inorganics are highly stable, but rarely exhibit CPL emission with high high dissymmetric factor (g_{lum}) value because of their structure rigidity and symmetry.

To obtain chirality, inorganics generally require the interaction with chiral organic ligands or matrix [6, 7]. For example, nano-size inorganics exhibit tortured lattice or overall shape induced by chiral ligands [8]. The dissymmetry of the tortured lattice or shape leads to the CPL emission or absorption, but suffers the low dissymmetry factor due to the limited size of the dissymmetric core. As reported, the inorganic nano-materials such as perovskite quantum dots (QDs), CdSe QDs or Ag clusters induced by chiral organic molecules showed a low g_{lum} value at only 10−3 magnitude in CPL emission and absorption [9–11]. Hybrid halide perovskites, emerging as the attractive semiconductors, achieved chirality with an advanced g_{lum} value of ~0.1 by introducing organic chiral components as A site [12, 13], but the g_{lum} value is still not insufficient to significantly differentiate the left-hand and right-hand CPL.

There is an alternative method for enlarging the chirality of inorganics by embedding the nano-materials into

✉ Zha Li
zhali@hust.edu.cn

✉ Liang Gao
highlight@hust.edu.cn

1 Wuhan National Laboratory for Optoelectronics, Huazhong University of Science and Technology, Wuhan 430074, China

2 School of Optical and Electronic Information, Huazhong University of Science and Technology, Wuhan 430074, China

3 International Health Care Center, National Center for Global Health and Medicine, Tokyo 162-8655, Japan

4 Hepato-Biliary-Pancreatic Surgery Division, Department of Surgery, The University of Tokyo Hospital, Tokyo 113-8655, Japan

5 Department of Urology, Union Hospital, Tongji Medical College, Huazhong University of Science and Technology, Wuhan 430074, China

6 Faculty of Materials Science and Chemistry, China University of Geosciences, Wuhan 430074, China

Published online: 31 May 2024

the matrix with twisted pattern. For example, carbon dots arranged in helical cellulose matrix can demonstrate visible CPL emission with a high g_{lum} value of 0.74 [14], much larger than that of organics or chiral ligand coated QDs. Because the cellulose matrix exhibits micro-meter scaled helical superstructure, much larger than the size of chiral QDs. However, the cellulose is organic material, insulating and unstable to heat and mechanical force, which is unfavorable for device fabrication. Nano-materials of semiconductors can be assembled in twisted structure to obtain high chirality leading by chiral organic ligands [15]. Thus, the large chirality mainly rely on the organic ligands or matrix, and pure inorganic counterparts are still challenging. Recently, through calcination, pure chiral inorganics could be obtained with outstanding chirality due to their chiral structure, with the higher stability than the organics [16–18]. There is also some other chiral inorganics fabricated by using porous silica as template [19]. However, these chiral inorganics were all metal oxides and only presented CPL absorption or CD signals, no CPL emission. We proposed to use these chiral hard templates to transfer the chirality to other inorganic semiconductors for CPL emission and detection.

Metal oxides are commonly used inorganics in optoelectronic device and, by our literature review, only 4 metal oxides, including ZnO, CuO, SnO_2 and TiO_2, were reported as chiral films [16, 17, 20, 21]. Among them, the chiral ZnO film possesses the highest dissymmetry factor with the lowest cost [16]. Here, we chose the chiral ZnO film as template to introduce CPL emission from $CsPbBr_3$ film and to enable CPL detection by PbS QDs. The precursor solution of $CsPbBr_3$ was simply spin-coated and annealed on the chiral ZnO template. The $CsPbBr_3$ layer succeeded the chiral structure directly from the ZnO template and exhibited strong CPL emission with a g_{lum} value of 0.41. This method is also available for other inorganic materials like PbS QDs, whose precursor solution was also spin-coated on the ZnO template with circular dichroism (CD signal at absorption range. The PbS QDs/ZnO film was assembled into photodetector and showed the ability of distinguishing left-/right-handed CPL at 780 nm with gdetect value around 0.4. Our method is universal for various semiconductors, which may open the gate to develop CPL emission and detection devices.

2 Results and discussion

We synthesized chiral ZnO film on FTO and silica substrates as the reported procedure [16]. As illustrated in Fig. 1a, zinc acetate was used as Zn source and the natural chiral amino acid was used as symmetric-breaking agent to direct the chiral structure. After calcination at 600 °C for 6 h, the ZnO film looks semi-transparent (Fig. 1b) and exhibits the helical and porous structure as shown in SEM images (Figs. 1c and d). Regarding to the report, the hierarchy structure of ZnO leads to high optical activity and outstanding circular dichroism (CD) spectrum, which comes from the twisted crystalline structure [16]. The absorption spectrum and the CD spectrum of the obtained ZnO films are presented in Figs. 1e and f, showing CD over 2000 mdeg from 350 to 400 nm consistent with the literature. The X-ray diffraction (XRD) pattern indicates the typical ZnO crystalline peaks in Fig. 1g.

We dropped the $CsPbBr_3$ precursor solution onto the ZnO film for 5 s incubation before the spin-coating. The morphology of ZnO is imprinted onto the $CsPbBr_3$ layer with or without excessive reagents remaining as shown in Fig. 2a. The high-speed (8000 r/min) spin-coating could remove the excessive reagents and the $CsPbBr_3$ that attached to the surface of the ZnO pores as a thin layer. The thin $CsPbBr_3$ inherits the geometric shape of ZnO, obtaining the twisted crystalline structure and demonstrating the chirality (Figs. 2b, S1a and b). If spin-coating at slow speed (3000 r/min), the thick $CsPbBr_3$ covers all over the ZnO structure (Fig. 2c). The g_{lum} value is defined by Eq. (1).

$$g_{lum} = \frac{2\left|PL_r - PL_l\right|}{\left|PL_r + PL_l\right|}, \tag{1}$$

where PL_r is right-hand photoluminescence (PL) and PL_l is left-hand PL. The thin $CsPbBr_3$ exhibits the CPL emission at 510 nm with g_{lum} value around 0.41 (Fig. 2d), while the thick $CsPbBr_3$ exhibits the CPL emission at 530 nm with decreased g_{lum} value around 0.26 (Fig. 2e). In the thick film, the excessive $CsPbBr_3$ is achiral and thus only contributes to the non-handed PL, which decreases the g_{lum} factor.

The PL of ZnO is too low compared with the PL of $CsPbBr_3$/ZnO as shown in Fig. S2. The chiral $CsPbBr_3$/ZnO film exhibits the CPL emission at around 520 nm, attributed to the electron transition from conduction band to valence band of $CsPbBr_3$ [19]. Referring to the chiral inorganics like TiO_2, ZnO and CuO, the optical activity of $CsPbBr_3$ is supposed to be the electronic transition based optical activity (ETOA) [16, 17, 22]. As the $CsPbBr_3$ film succeeds to the structure from the chiral ZnO film, the $CsPbBr_3$ film demonstrates chiral structure, offerring the anisotropic environment for the electron transition. The Coulomb interaction under the anistropic field impacts the electron transition of $CsPbBr_3$ from the valence band to the conduction band and the reverse process.

According to the previous report, the hierarchical structure of the ZnO substrate enabled the high chirlity, including three levels: the primary helical ZnO crystalline structures within the nanoplates, the secondary helical structure of the stacks of the nanoplates, the tertiary assemblies by several stacks. To succeed the chirality of the ZnO substrate, it is plausible that the $CsPbBr_3$ film exists in the rather limited

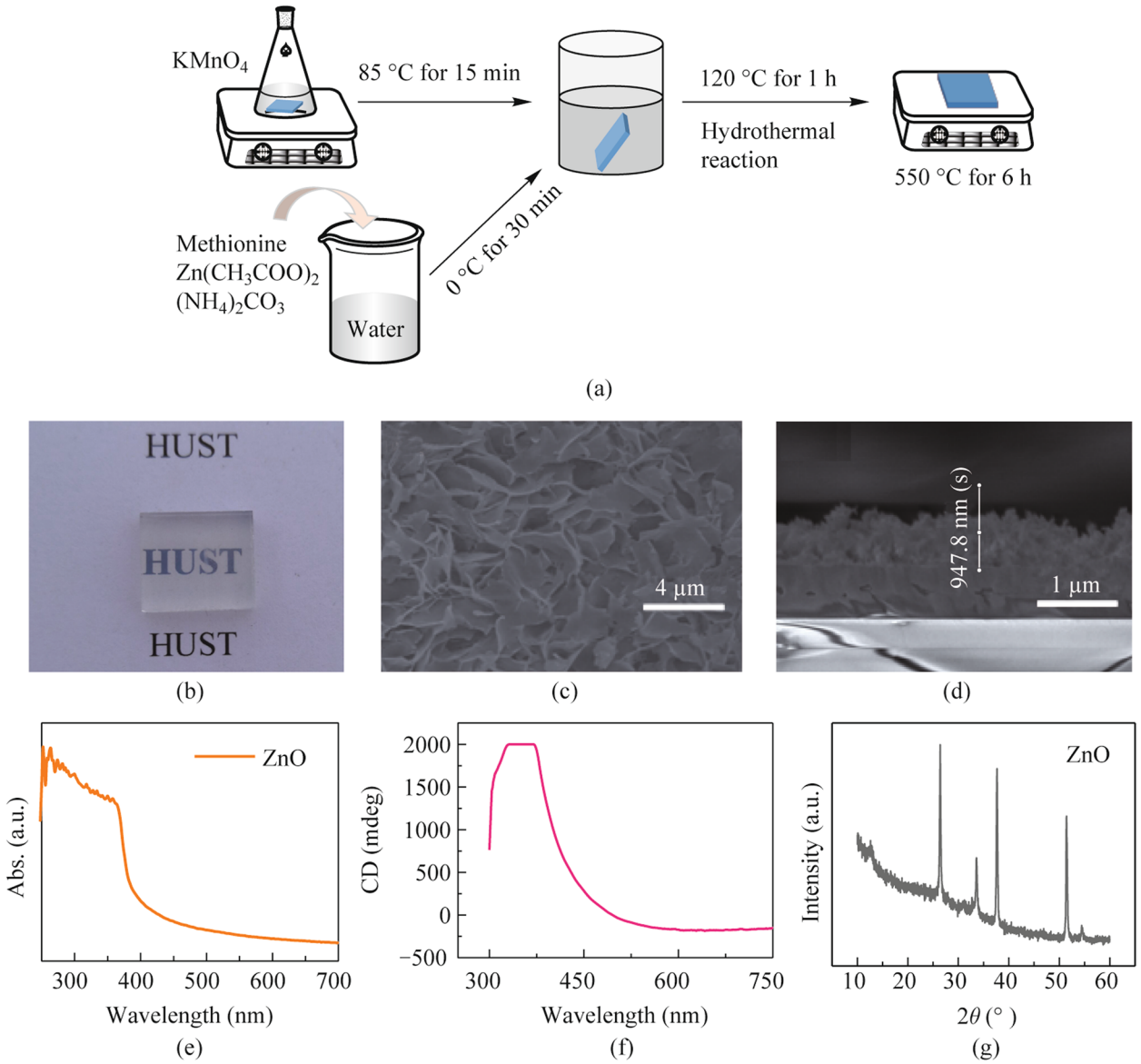

Fig. 1 **a** Synthesis of chiral porous ZnO film on substrate. **b** Photo-graph of the obtained ZnO film on substrate. **c** Surface and **d** cross-section images of ZnO by SEM. **e** UV-Vis absorption and **f** CD spectrum of ZnO film. **g** XRD pattern of ZnO film

inter-space between the ZnO nanoplates to succeed the similar hierarchical structure, meanwhile $CsPbBr_3$ film possesses rather small thickness.

To further investigate the ETOA mechanism, we modified the coating process. We span the ZnO film at high speed first and then dropped the $CsPbBr_3$ solution onto the furface of the ZnO film. Thus, the resulted morphology is the smooth $CsPbBr_3$ layer lying on the ZnO film as indicated in SEM image (Fig. S3). The reason is that the pore size of the ZnO film is small and the surface tension delays the $CsPbBr_3$ solution entering the pores. During the spin-coating process, the $CsPbBr_3$ solution directly crystallizes over the pores and forms smooth $CsPbBr_3$ film. If the scattering or reflection mechanism works, the chiral ZnO film should have worked as chiral filter and still lead to CPL emission. But the result did not show any CPL emission from $CsPbBr_3$ film, denying this mechanism and favoring the electronic transition-based mechanism.

In the thin $CsPbBr_3$ film case, the $CsPbBr_3$ precursor solution enters into the pores of ZnO film. By high speed spin-coating, the excessive solution was removed and only the small volume parts attached to the ZnO surface and grew into crystallites in the rather confined space nearby. The resulted $CsPbBr_3$ crystallites are rather small, directly attach to ZnO surface and follow the helical spatial arrangement, leading to the chiral structure and optical activity. The CPL

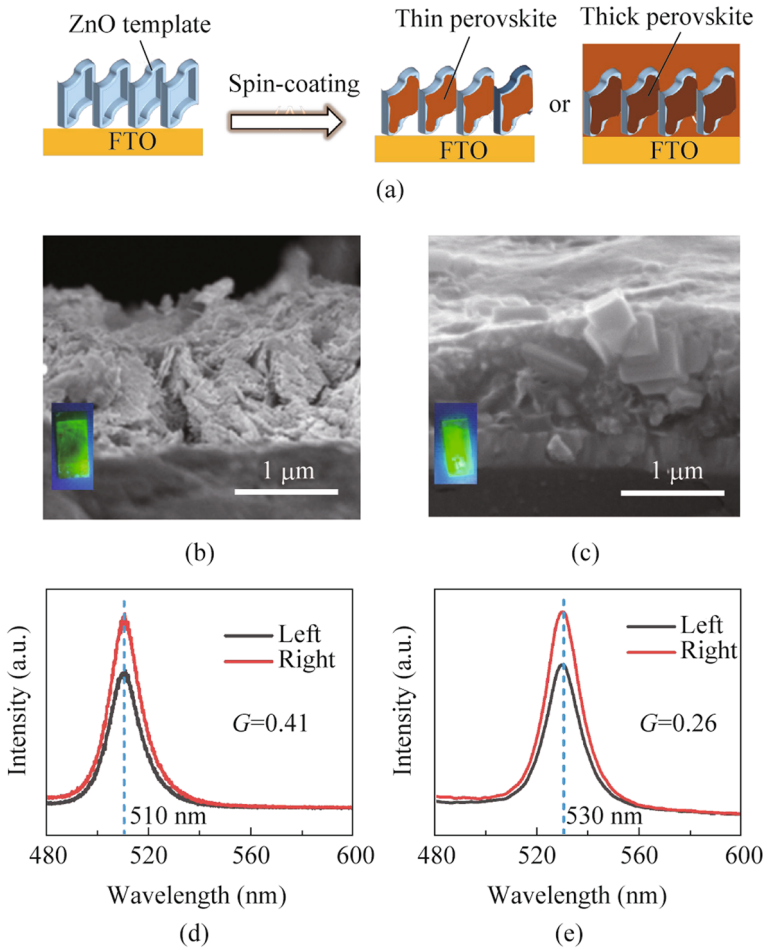

Fig. 2 **a** Scheme of spin-coating perovskite on porous ZnO film. The porous structure is imprinted by thin or thick perovskite. Cross-section scanning electron microscope (SEM) images of **b** thin and **c** thick perovskite film on porous ZnO. Insert, the perovskite/ZnO under UV-irradiation. Left-hand and right-hand CPL spectra of **d** thin and **e** thick perovskite film on the chiral ZnO film

emission exhibits a little hypochromic shift, mostly likely due to the confined size of crystallites.

For the thick $CsPbBr_3$ film, less spin-coating speed retained more precursor solution in the pores or over the ZnO film. More $CsPbBr_3$ crystallites are supposed to form freely in the pores, or even over the whole ZnO film, without attaching to the ZnO surface nor spatial confinement. Since they do not attach to the ZnO surface tightly nor follow the chiral ZnO structure, these parts exhibit no contribution to the chirality and lead to decreased g_{lum} value. By experiment, when the thickness over 2 μm, no CPL emission occurs and g_{lum} value is zero (Fig. S4). Without the spatial confinement, the PL spectrum from thick $CsPbBr_3$ exhibits the bathochromic shift, which also supports our hypothesis. In addition, the CD spectra detected from different sides and rotation angles do not show obvious difference, which is supposed to eliminate the influence of linearly birefringence and linearly dichroism [17] (Fig. S5).

According to this electronic transition-based mechanism, other inorganics are also supposed to be applicable. We chose achiral PbS QDs as an active semiconductor on the chiral ZnO film for CPL detection. The PbS QDs solution was spin-coated on the ZnO film and the PbS QDs/ZnO thin film was obtained with the configuration in Fig. 3a. The PbS QDs/ZnO film exhibits the CD signals as shown in Fig. 3b, where the peak value is near to the absorption edge and attributed to the ETOA mechanism. The PbS QDs are aligned along the ZnO surface and form the helical structure film. In this film, the anisotropic electric field impact the electron transition process, including the exciton occurrence and separation, and the corresponding photo-current. We applied the chiral PbS QDs/ZnO film as a photodetector and measured by a home-made photo-detection system (Fig. S6). The 780 nm light-emitting diode was chosen as light source and modulated by the polarizer and 1/4 wave plate to generate the left- and right-handed CPL. The PbS QDs/ZnO film shows distinct response to left- and right-handed CPL

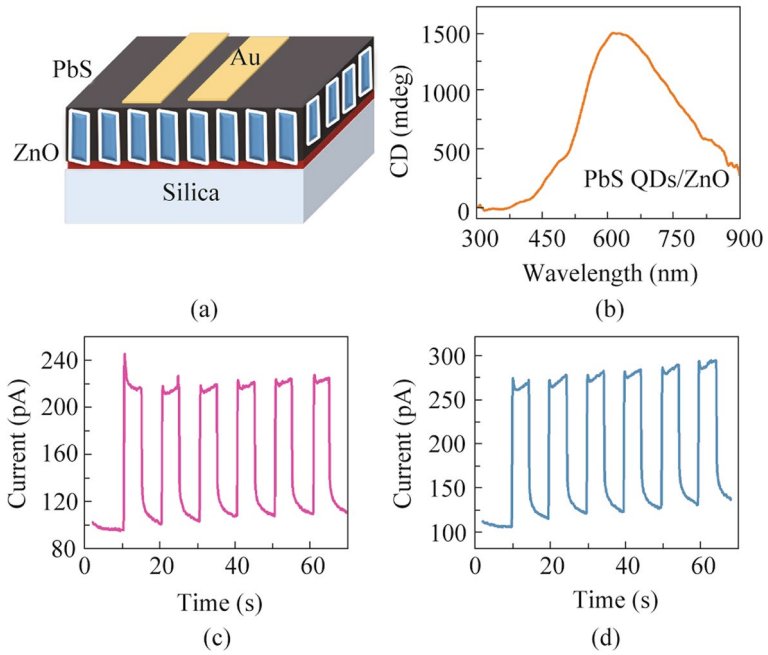

Fig. 3 **a** Schematic illustration of photodetector of Au/PbS QDs/ZnO/silica. **b** The CD spectrum of the PbS QDs film on porous ZnO. The current–time curve of the photodetector under the **c** left-handed and **d** right-handed 780 nm irradiation with gdetect value calculated as 0.4

irradiation with the same power density in Fig. S7 (g_{detect}= 0.7). For CPL detection, the g_{detect} value is defined by Eq. (2) as follows:

$$g_{detect} = \frac{2|PC_r - PC_l|}{|PC_r + PC_l|}, \quad (2)$$

where PC_r and PC_l are the net photocurrents to right- and left-handed light, respectively. The response speed is rather slow, likely due to the interaction between ZnO and PbS QDs (Fig. S7). To enhance the response speed, we deposited an Al_2O_3 layer of 3 nm thickness on the ZnO film as insulator by atomic layer deposition (ALD) before spin-coating PbS QDs. The Al_2O_3 layer blocked the interaction between ZnO and PbS QDs, but retained the chiral structure of the ZnO film because of conformal coating of Al_2O_3. Consequently, the response speed is enhanced greatly and the CPL distinction remains significant with gdetect value around 0.4 as shown in Figs. 3c and d.

In summary, we have demonstrated a universal method to transfer chirality from chiral porous inorganic hard template to other achiral inorganic semiconductors. The resulted semiconductors succeed the chiral structure and high chiral activity based on electronic transition with the high dissymmetric value. In this study, we used the chiral ZnO film as hard template and coated $CsPbBr_3$ and PbS QD as the active semiconductors. The chiral $CsPbBr_3$ film exhibit CPL emission at 520 nm with g_{lum} up to 0.4. The PbS QDs film distinguish CPL at 780 nm with gdetect up to 0.4. We prove that the chiral porous hard template endows the chirality to other semiconductors for chiral sensitive applications. The ETOA mechanism is responsible for the transferred chirality and the wavelength is tunable referring to the band gap.

3 Experimental section

3.1 Reagents

Lead bromide ($PbBr_2$, 98%), lead iodide (PbI_2, 99%) and cesium bromide (CsBr, 99%) were purchased from Aladdin. DMF, zinc acetate dihydrate ($Zn(OAC)_2{\cdot}2H_2O$), Methionine, $(NH_4)_2CO_3$, $KMnO_4$ and butanol were purchased from Sinopharm Chemical Reagent Co. Ltd. All reagents were directly used without any further purification.

3.2 Fabrication of chiral porous ZnO film

FTO or silica substrate was sequentially rinsed by detergent solution, water, acetone and ethanol in ultrasonic bath for 10 min. Then the clean substrate was incubated in 20 mL 10 mmol/L $KMnO_4$ solution/50 µL of butanol mixture at 85 °C for 15 min for activation. The resulted FTO was yellowish transparent. 2 mmol methionine and 3 mmol $Zn(CH_3COO)_2{\cdot}2H_2O$ were mixed and dissolved in 25 mL water solution with stirring. 1 mmol $(NH_4)_2CO_3$ was added and stirred in ice-water bath for 0.5 h. Then the activated substrate was placed in 25 mL Teflonlined autoclave with

immersion into the suspension to react at 120 °C for 1 h. Then the substrate with ZnO film was washed by water and ethanol for several times. After dried in the air, the ZnO/ substrate was followed by slow heating procedure of 6 h to 550 °C and calcination for 6 h.

3.3 $CsPbBr_3$ spin-coating

25 mmol/L CsBr and $PbBr_2$ were dissolved in DMSO by long time stirring as $CsPbBr_3$ precursor solution. The spin-coating speed was adapted from 3000 to 8000 r/min. Then, to enhance the brightness, we dropped 10 mg/mL MABr/ isopropanol on the film and spin-coated at 5000 r/min for 30 s. The films were dried in air at 100 °C on the hot-plate.

3.4 PbS QD synthesis

Following the previous protocol, 0.9 g PbO, 2.9 g oleic acid (OA) and 20 mL octadecene (ODE) were degassed at 85 °C with 6 h stirring. The Pb-source solution became colorless transparent. Then, 320 μL hexamethyldisilathiane (TMS) dissolved in 10 mL degassed ODE was quickly injected into the Pb-source solution at 85 °C and heated for 10 s. Then the heating mantle was directly removed and the mixture naturally cooled down to the room temperature. The PbS QDs were washed and purified by precipitation.

3.5 Al_2O_3 atomic-layer-deposition (ALD)

The ALD is executed by ASM Pulsar2000™ ALD module to grow the Al_2O_3 layer. The Al_2O_3 was grown by alternating pulses of $Al(CH_3)_3$ and H_2O with the carrier gas flow of nitrogen. By controlling the number of ALD cycles, the thicknesses 30 Å were set with the reaction temperature of 300 °C.

3.6 CPL emission measurement

CPL emission measurement was carried out on a homemade Raman spectrometer system with a 405 nm linearly polarized laser light source at 0.1 μW. The CPL passed through a quarter-wave plate followed by a polarizer. The transmission was recorded by a CCD instrumentation (Symphony II, Horiba). The schema of the system was illustrated in the supporting information (Fig. S8).

3.7 Characterization

The scanning electron microscopic measurement (SEM) was carried out by FEI Nova Nano 450 SEM. TEM observations were performed on a Tecnai G2 20U-TWIN machine at 300 kV. The XRD measurement was executed on Philips X pert pro MRD diffractometer with Cu Kα radiation. The CD spectrum were obtained using JASCO J-810 spectrophotometers.

Supplementary Information The online version contains supplementary material available at https://doi.org/10.1007/s12200-024-00120-8.

Acknowledgements This work was supported by the National Natural Science Foundation of China (Grant No. 61904065), the National Key R&D Program of China (No. 2016YFB070700702) and the National Postdoctoral Program for Innovative Talent (No. BX20190127). The authors thank the Analytical and Testing Center of HUST and the facility support of the Center for Nanoscale Characterization and Devices (CNCD), WNLO-HUST. The authors thank the Prof. Yanqing Wu and Xuefei Li group for the help in the experiment of ALD.

Authors' contributions ZL and LG carried out the design of the experiments and discussed the mechanism. WL and DL carried out the CPL emission measurement and the discussion of the results. WT, HL, and HS participated in the CPL absorption measurement and the discussion of the results. LG, CC, and JT offered the finacial aids and drafted the manuscript. All authors read and approved the final manuscript.

Availability of data and materials The data that support the findings of this study are available from the corresponding author, upon reasonable request.

Declarations

Competing interests There are no conflicts of interest to declare.

References

1. Huo, S.W., Duan, P.F., Jiao, T.F., Peng, Q.M., Liu, M.H.: Self-assembled luminescent quantum dots to generate full-color and white circularly polarized light. Angew. Chem. Int. Ed. **56**(40), 12174–12178 (2017)
2. Song, F.Y., Wei, G., Jiang, X.X., Li, F., Zhu, C.J., Cheng, Y.X.: Chiral sensing for induced circularly polarized luminescence using an Eu(III)-containing polymer and D- or L-proline. Chem. Commun. (Camb.) **49**(51), 5772–5774 (2013)
3. Yang, Y., Da Costa, R.C., Fuchter, M.J., Campbell, A.J.: Circularly polarized light detection by a chiral organic semiconductor transistor. Nat. Photonics **7**(8), 634–638 (2013)
4. Stanciu, C.D., Hansteen, F., Kimel, A.V., Kirilyuk, A., Tsukamoto, A., Itoh, A., Rasing, T.: All-optical magnetic recording with circularly polarized light. Phys. Rev. Lett **99**(4), 047601 (2007)

5. Sanchez-Carnerero, E.M., Agarrabeitia, A.R., Moreno, F., Maroto, B.L., Muller, G., Ortiz, M.J., de la Moya, S.: Circularly polarized luminescence from simple organic molecules. Chemistry **21**(39), 13488–13500 (2015)
6. Ma, W., Xu, L., de Moura, A.F., Wu, X., Kuang, H., Xu, C., Kotov, N.A.: Chiral inorganic nanostructures. Chem. Rev. **117**(12), 8041–8093 (2017)
7. Zhao, T.H., Han, J.L., Jin, X., Liu, Y., Liu, M.H., Duan, P.F.: Enhanced circularly polarized luminescence from reorganized chiral emitters on the skeleton of a zeolitic imidazolate framework. Angew. Chem. Int. Ed. **58**(15), 4978–4982 (2019)
8. Ben-Moshe, A., Wolf, S.G., Sadan, M.B., Houben, L., Fan, Z.Y., Govorov, A.O., Markovich, G.: Markovich, G.: Enantioselective control of lattice and shape chirality in inorganic nanostructures using chiral biomolecules. Nat. Commun. **5**(1), 4302 (2014)
9. Liu, C., Li, T., Abroshan, H., Li, Z.M., Zhang, C., Kim, H.J., Li, G., Jin, R.C.: Chiral Ag-23 nanocluster with open shell electronic structure and helical face-centered cubic framework. Nat. Commun **9**(1), 744 (2018)
10. Varga, K., Tannir, S., Haynie, B.E., Leonard, B.M., Dzyuba, S.V., Kubelka, J., Balaz, M.: CdSe quantum dots functionalized with chiral, thiol-free carboxylic acids: unraveling structural requirements for ligand-induced chirality. ACS Nano **11**(10), 9846–9853 (2017)
11. Shi, Y.H., Duan, P.F., Huo, S.W., Li, Y.G., Liu, M.H.: Endowing perovskite nanocrystals with circularly polarized luminescence. Adv. Mater **30**(12), 1705011 (2018)
12. Wang, C.T., Chen, J.Q., Xu, P., Yeung, F., Kwok, H.S., Li, G.J.: Fully chiral light emission from CsPbX3 perovskite nanocrystals enabled by cholesteric superstructure stacks. Adv. Funct. Mater **29**(35), 1903155 (2019)
13. Ma, J.Q., Fang, C., Chen, C., Jin, L., Wang, J.Q., Wang, S., Tang, J., Li, D.H.: Chiral 2D perovskites with a high degree of circularly polarized photoluminescence. ACS Nano **13**(3), 3659–3665 (2019)
14. Zheng, H.Z., Ju, B., Wang, X.J., Wang, W.H., Li, M.J., Tang, Z.Y., Zhang, S.X.A., Xu, Y.: Circularly polarized luminescent carbon dot nanomaterials of helical superstructures for circularly polarized light detection. Adv. Opt. Mater **6**(23), 1801246 (2018)
15. Sang, Y.T., Han, J.L., Zhao, T.H., Duan, P.F., Liu, M.H.: Circularly polarized luminescence in nanoassemblies: generation, amplification, and application. Adv. Mater. **32**(41), 1900110 (2020)
16. Duan, Y.Y., Han, L., Zhang, J.L., Asahina, S., Huang, Z.H., Shi, L., Wang, B., Cao, Y.Y., Yao, Y., Ma, L.G., Wang, C., Dukor, R.K., Sun, L., Jiang, C., Tang, Z.Y., Nafie, L.A., Che, S.N.: Optically active nanostructured ZnO films. Angew. Chem. Int. Ed. **54**(50), 15170–15175 (2015)
17. Duan, Y.Y., Liu, X., Han, L., Asahina, S., Xu, D.D., Cao, Y.Y., Yao, Y., Che, S.N.: Optically active chiral CuO "nanoflowers". J. Am. Chem. Soc. **136**(20), 7193–7196 (2014)
18. Gao, C.B., Che, S.A.: Organically functionalized mesoporous silica by co-structure-directing route. Adv. Funct. Mater. **20**(17), 2750–2768 (2010)
19. Duan, Y.Y., Che, S.N.: Electron transition-based optical activity (ETOA) of achiral metal oxides derived from chiral mesoporous silica. Chemistry **19**(32), 10468–10472 (2013)
20. Shen, Q., Mao, W.T., Han, L., Duan, Y.Y., Che, S.A.: Chiral mesostructured SnO_2 films with tunable optical activities. Opt. Mater. **94**, 21–27 (2019)
21. Zhang, F., Ai, J., Ding, K., Duan, Y., Han, L., Che, S.: Synthesis of chiral mesostructured titanium dioxide films. Chem. Commun. (Camb.) **56**(35), 4848–4851 (2020)
22. Liu, S.H., Han, L., Duan, Y.Y., Asahina, S., Terasaki, O., Cao, Y.Y., Liu, B., Ma, L.G., Zhang, J.L., Che, S.A.: Synthesis of chiral TiO_2 nanofibre with electron transition-based optical activity. Nat. Commun **3**(1), 1215 (2012)